Simulation-based decision-making framework for sustainable intermodal transport including next-generation freight electric multiple-units

Progress in Organic Coatings 217 (2026) 110218

Contents lists available at ScienceDirect

Progress in Organic Coatings

journal homepage: www.elsevier.com/locate/porgcoat

From lignin to high performance coatings: UV curing of bisguaiacol-derived resins and hybrid organic–inorganic coatings

Nicola Porcelli [a], Matteo Bergoglio [b], Niccolò Braidi [a], Fabrizio Roncaglia [a], Marco Sangermano [b,*]

[a] Department of Chemical and Geological Sciences, University of Modena and Reggio Emilia, Via Giuseppe Campi 103, Modena, 41125, Italy
[b] Dipartimento Scienza Applicata e Tecnologia, Politecnico di Torino, Corso Duca degli Abruzzi 24, 10129, Torino, Italy

ARTICLE INFO

Keywords:
Photopolymerization
Bionased monomers
Bisguaiacol F
Lignin derivatives

ABSTRACT

This study reports the development of sustainable UV-curable coatings based on lignin-derived aromatic building blocks. Bisguaiacol F (BGF) isomers obtained from vanillyl alcohol and guaiacol were functionalized to produce bisguaiacol-F-diacrylate (BGF-DEDA) and bisguaiacol-F-diglycidyl ether (BGF-DGE), which were evaluated in both pristine formulations and hybrid systems containing tetraethyl orthosilicate (TEOS). The photopolymerization behavior of the formulations was investigated, revealing different reactivity trends depending on the curing mechanism. The use of dual-curing strategies enabled effective formation of an inorganic silica network. Dynamic mechanical thermal analysis (DMTA) and field emission scanning electron microscopy (FESEM) confirmed the in-situ generation and homogeneous dispersion of silica nanoparticles, which significantly restricted polymer chain mobility. As a result, hybrid materials exhibited notable improvements in thermomechanical performance, with glass transition temperatures reaching up to 106 °C and surface hardness values up to 8H in epoxy-based coatings. Overall, these results demonstrate the potential of lignin-derived aromatic platforms for designing high-performance bio-based hybrid coatings with tunable properties, offering promising prospects for advanced protective coating applications.

1. Introduction

Growing awareness of climate change and the progressive depletion of fossil-based resources has intensified research efforts toward the development of sustainable alternatives to petroleum-derived polymers. In this context, the replacement of conventional petrochemical feedstock with renewable and bio-based building blocks has become a key objective, particularly in the field of polymeric coatings, where large volumes of materials are produced and consumed annually. The design of sustainable precursors for coating applications is therefore of considerable interest, as highlighted in recent reviews addressing green strategies for polymer synthesis and processing [1–5].

Among advanced coating technologies, ultraviolet (UV) curing has emerged as a highly attractive approach due to its low environmental footprint. UV-curable systems are typically solvent-free, exhibit rapid curing rates, and require relatively low energy input, resulting in significant reductions in processing time and energy consumption [6,7]. These advantages make UV curing particularly appealing for industrial applications. Acrylates, methacrylates, and epoxy resins remain the most widely employed chemistries in UV-curable formulations, owing to their high reactivity and tunable material properties under radical and cationic photopolymerization mechanisms.

Over the past decades, substantial progress has been made in the development of bio-based and renewable polymer precursors suitable for UV-curing applications. Numerous studies have demonstrated the feasibility of replacing fossil-derived monomers with bio-sourced alternatives while maintaining competitive performance [8]. To replace petrochemical monomers, cyclic monoterpene-based acrylates have been proposed since they combine good mechanical properties with decreased volatility [9]. The synthesis of a bio-based acrylated polyol derived from castor oil glycidyl ether and its formulation into a UV-curable coating resin were recently reported, showing interesting properties in terms of corrosion protective coatings [10]. Recent review highlighting bio-based acrylic resins, including acrylated tannic acid systems and other renewable monomers used to enhance adhesion and corrosion protection in coatings [11].

* Corresponding author.
E-mail address: marco.sangermano@polito.it (M. Sangermano).

https://doi.org/10.1016/j.porgcoat.2026.110218
Received 6 March 2026; Received in revised form 2 April 2026; Accepted 23 April 2026

Epoxidised vegetable oils represent one of the most commercially established classes of bio-based epoxidised resins, benefiting from the abundance and accessibility of unsaturated fatty acid chains that can be readily functionalized with epoxy groups. These systems have been widely investigated in our group [12–14]. In particular, epoxidised linseed oil and cardanol-based resins have been investigated as renewable starting materials for coating applications [15]. Further studies have also demonstrated the successful use of bio-renewable epoxy monomers in cationic photopolymerization, highlighting the possibility of tailoring the properties of the resulting crosslinked networks through selection of the monomer structure [16].

Despite their advantages, triglyceride-based epoxy resins suffer from intrinsic structural limitations. The presence of long aliphatic chains typically leads to low cross-link densities and highly flexible polymer backbones, which often translate into inadequate thermomechanical performance, particularly in applications requiring high stiffness, thermal stability, or dimensional integrity [17,18].

To overcome these limitations, alternative bio-based building blocks with more rigid molecular architectures have been explored. Isosorbide, a bicyclic compound derived from glucose, has attracted significant attention due to its rigid heterocyclic structure, which can impart high glass-transition temperatures and improved mechanical properties upon functionalization and curing [19,20]. However, the strong hydrophilicity of isosorbide-based resins remains a major drawback, limiting their applicability in moisture-sensitive environments.

Other promising renewable platforms include itaconic acid [21–24], both of which can be derived from biomass and have been successfully employed in the synthesis of epoxy resins. These molecules offer the advantage of incorporating unsaturation or aromatic functionality, enabling the formation of crosslinked networks with enhanced thermal and mechanical properties. Similarly, cellulose-derived furan-based epoxy resins have been reported as high-performance bio-based alternatives, capable of achieving elevated glass-transition temperatures and high storage moduli at ambient conditions due to their rigid aromatic-like backbone [25–27].

Within this framework, lignin-derived aromatic compounds represent an especially appealing class of renewable feedstocks, as they combine bio-based origin with inherent structural rigidity and large availability, also as waste feedstock valorization. In the present work, we focus on precursor resins obtained through the aromatic condensation of vanillyl alcohol and guaiacol, both readily accessible from lignin depolymerization pathways [28], leading to the formation of bisguaiacol F (BGF) isomers, as schematized in Fig. 1.

BGF mimics the 4,4′-methylenediphenol structure, which is the structural motif of bisphenol F (BPF) and all bisphenolic analogues. Numerous syntheses of BGs were reported in the literature, differing mainly in the degree of substitution of the aromatic rings and the nature of the bridging element between them. The common feature among

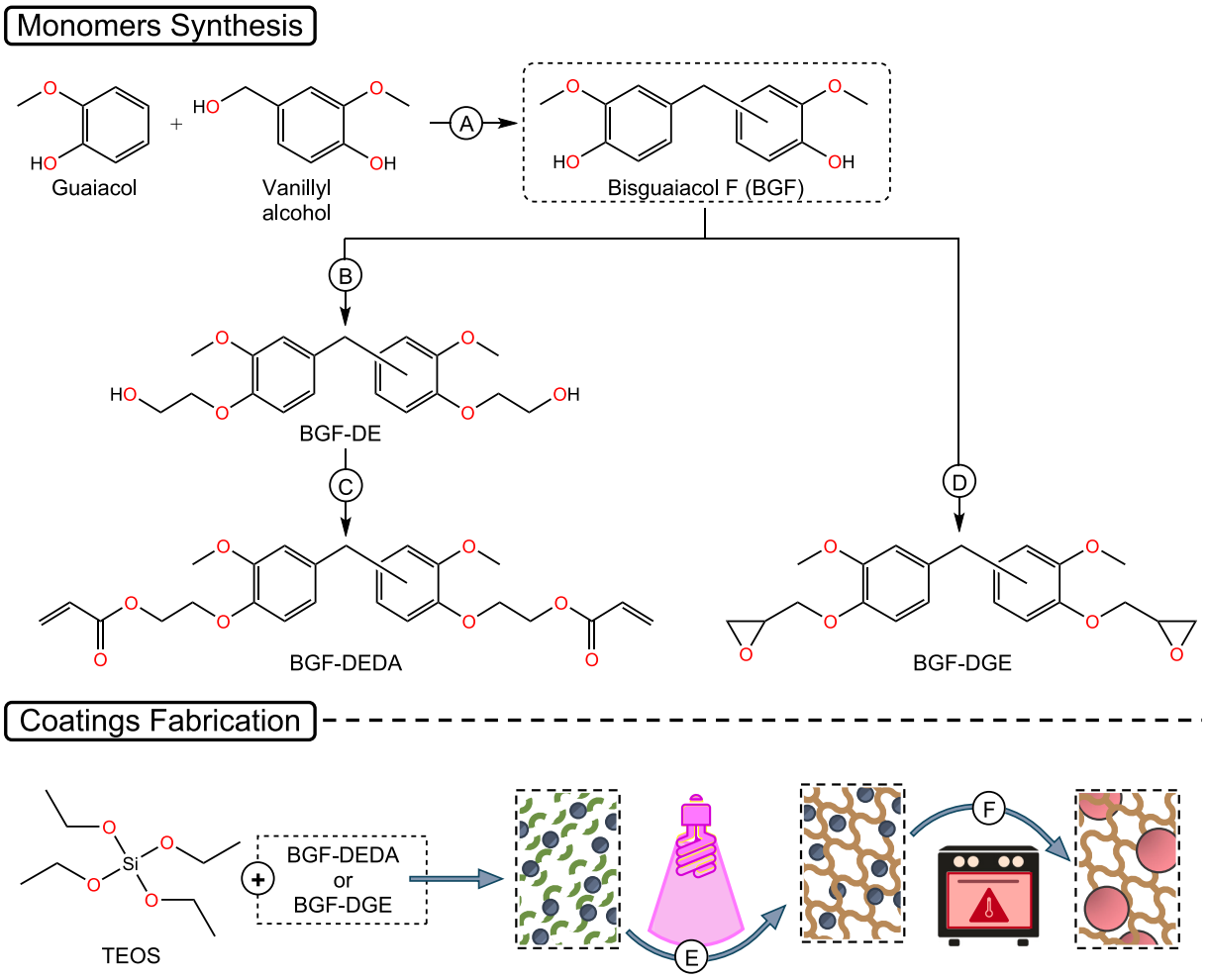

Fig. 1. Schematic overview of the synthetic and fabrication routes followed, *upper* and *lower* schemes respectively. Synthesis of bisguaiacol F derivatives. Reaction pathway to BGF-DEDA. A) Guaiacol (8.0 eq.), SSANa (0.2 eq.), 80 °C, 3 h; B) EC (3.0 eq.), K_2CO_3 (0.2 eq.), 160 °C, 6 h; C) AcrCl (2.4 eq.), TEA (3.0 eq.), DCM, 0 °C, 1 h, RT, 2 h. 2) Reaction pathway to BGF-DGE. D) ECH (10.0 eq.), TEAB (0.1 eq.), 60 °C, 2 h; NaOH (4.0 eq.), RT, overnight. E) Photoinitiator (2 phr), mixing, UV-curing (3 min, 170 mW/cm^2); F) 160 °C, 2 h. Please refer to the experimental section for a detailed description of the methods.

structures are the two aromatic rings that impart structural rigidity, giving the bisphenolic molecule the stacking characteristics which are reflected in the excellent mechanical performance of the derived polymers. Furthermore, it was shown that the presence of *ortho*-substituent methoxy groups on the aromatic rings greatly reduces the toxicity commonly associated with bisphenolic analogues [29,30], thus making them ideal candidates for replacing BPA in its various applications. The synthesis of these BPA analogues follows a common pattern: they are acid-catalyzed electrophilic aromatic substitution reactions, often conducted under mild conditions and require excess substrate to prevent isomerization and oligomerization phenomena. BGF is, indeed, the most studied of all BG derivatives [31–33]. It is both the cheapest to produce and has the most straightforward synthesis. Despite its history in synthesis, it is yet to be studied in the context of coating applications. Thus, the compound was synthesized and accordingly functionalized with acrylates and epoxy groups to tailor the needs of the various photopolymerization processes.

To enhance the final thermo-mechanical properties of the UV-cured coatings, a strategy previously proposed by our group was adopted [26]. Specifically, a hybrid organic–inorganic network was developed via a sol–gel process, using tetraethoxysilane (TEOS) as the precursor for the inorganic phase, via a dual UV-thermal curing process. The process involves a series of hydrolysis and condensation reactions of hydrolysable multifunctional alkoxysilane. The incorporation of the sol–gel–derived inorganic domains within the UV-curable organic matrix is expected to improve coating performance by increasing mechanical robustness and thermal stability. At the same time, this approach is designed to preserve and valorize the intrinsic sustainability benefits of lignin-derived aromatic components, effectively combining renewable feedstocks with the high performance required for advanced UV-curable coating systems.

This work introduces, for the first time, the use of lignin-derived bisguaiacol F (BGF) as a multifunctional platform for UV-curable coating systems, addressing the current lack of studies on its application in this field. Unlike conventional bio-based epoxy resins derived from triglycerides, which suffer from limited thermo-mechanical performance, the rigid aromatic structure of BGF enables the development of high-performance networks. Furthermore the dual functionalization of BGF into both acrylate and epoxy resins, allowing comparison of radical and cationic photopolymerization pathways, combined with the integration of a sol–gel-derived inorganic phase to form hybrid organic–inorganic coatings. This synergistic approach enables the design of largely bio-based UV-curable materials with enhanced thermal and mechanical properties, bridging the gap between sustainability and high-performance coating applications.

2. Materials and methods

2.1. Materials

Guaiacol (Sigma-Aldrich, 99%), vanillyl alcohol (VA) (Sigma-Aldrich, 98%), ethylene carbonate (EC) (Fluka, >99%), triethylamine (TEA) (Sigma-Aldrich, for synthesis), acryloyl chloride (AcrCl) (Sigma-Aldrich, 97%), epichlorohydrin (ECH) (Tokyo Chemical Industry, >99%), tetraethyl ammonium bromide (TEAB) (Sigma-Aldrich, for synthesis), silica gel (Millipore, 0.063–0.200 mm mesh), dichloromethane (DCM) (Sigma-Aldrich, 99.5%), ethyl acetate (EtOAc) (Sigma-Aldrich, 99.5%), petroleum ether (PE) (Sigma-Aldrich, b.p. = 40–60 °C), diethyl ether (DE) (Sigma-Aldrich, 98%), methanol (MeOH) (Sigma-Aldrich, 99%), potassium carbonate (Riedel-de Haen, >99%), sodium carbonate (Sigma-Aldrich, 99.5%), concentrated H_2SO_4 (Scharlau, 95–97%), and NaOH (Carlo Erba, >99%), phenylbis(2,4,6-trimethylbenzoyl)phosphine oxide (Sigma-Aldrich, 97%), triarylsulfonium hexafluoroantimonate salts, mixed at 50 wt% solution in propylene carbonate (Sigma-Aldrich), tetraethyl orthosilicate (Sigma-Aldrich, 97%). All reagents and solvents were used as purchased without further purification.

2.2. BGF-DEDA and BGF-DGE synthesis

2.2.1. Preparation of silica sulfuric acid sodium salt (SSANa, 3.0 mmol/g)

$NaHSO_4$ (2.34 M aqueous solution, 7.5 mL, 17.55 mmol) and SiO_2 (3.75 g) were inserted in a 25 mL round bottom flask containing a magnetic stirring bar, and the mixture was stirred for 15 min. Once evaporated to dryness at the rotavapor, the solid residue (free-flowing powder) was oven-dried at 130 °C overnight, giving SSANa (3.0 mmol/g) as a white powder (5.86 g).

2.2.1.1. Synthesis of bisguaiacol F (BGF). In a typical experiment, guaiacol (10 g, 80.6 mmol) and VA (1.55 g, 10.1 mmol) were inserted into a 50 mL round bottom flask. The suspension was heated to 80 °C while vigorously stirring, until complete dissolution of VA, then SSANa 3.0 mmol/g (0.67 g, 20.0 mol%) was added. The reaction mixture turned light purple over the course of one hour. Upon completed consumption of VA, monitored by thin layer chromatography (TLC) (DCM: MeOH = 90: 10 *v*/v), the reaction mixture was filtered to remove SSANa and the filter washed with DCM (10 mL). After removing the volatile fractions under reduced pressure, the crude product was first heated under reduced pressure to remove residual guaiacol through distillation (39 °C, 1.6 mbar). The residue was further purified through flash column chromatography (PE: DE = 80: 20 *v*/v, then PE: EA = 60: 40 *v*/v), affording BGF as a white solid (13.22 g, 66% yield).

^{1}H NMR (600 MHz, $CDCl_3$) δ (ppm): 6.86–6.64 (m, 6H, Ar—H), 5.59–5.41 (s, 2H, Ar-OH), 3.87–3.83 (m, 6H, Ar-OCH_3), 3.85–3.80 (bs, 2H, Ar-CH_2).

^{13}C NMR (600 MHz, $CDCl_3$) δ (ppm): 146.62, 145.65, 145.04, 144.06, 135.08, 133.48, 133.69, 122.72, 121.63, 120.18, 119.54, 115.18, 114.34, 111.47, 110.80, 108.77, 56.16, 56.01, 41.34, 41.10, 35.27.

2.2.1.2. Synthesis of BGF bis(2-hydroxyethyl) ether) (BGF-DE). BGF (1.00 g, 3.84 mmol), EC (1.014 g, 11.5 mmol), and K_2CO_3 (0.106 g, 0.77 mmol) were inserted into a 25 mL round bottom flask and heated to 160 °C for 6 h, under vigorous stirring. The reaction mixture turned light brown over the course of one hour. Upon complete consumption of BGF (monitored by TLC, DCM: MeOH = 90: 10 *v*/v), the reaction mixture was cooled to 100 °C and 2 M aqueous H_2SO_4 was added to neutralize K_2CO_3. The mixture was first stirred at 100 °C for 0.5 h, then it was cooled to room temperature. Once transferred to a separatory funnel, the mixture was diluted with EtOAc (50 mL) and washed with brine (5 × 25 mL). After drying over Na_2SO_4, the organic phase was filtered on a Gooch funnel and concentrated under reduced pressure. The so obtained dark red liquid BGF-DE (1.61 g, 96% yield), was used in the following without further purification.

^{1}H NMR (600 MHz, $CDCl_3$) δ (ppm): 6.88–6.66 (m, 6H, Ar—H), 4.17–4.07 (m, 4H, C-CH_2-O), 3.92–3.87 (m, 2H, Ar-O-CH_2-C), 3.87–3.77 (m, 8H, Ar-O-CH_3 + Ar-CH_2-Ar).

^{13}C NMR (600 MHz, $CDCl_3$) δ (ppm): 150.1, 149.7, 146.6, 146.5, 135.5, 135.3, 134.8, 134.7, 122.3, 121.2, 121.0, 120.9, 116.2, 115.5, 114.0, 112.7, 111.9, 72.7, 71.9, 69.6, 68.8, 61.8, 61.4, 56.0, 41.2.

2.2.1.3. Synthesis of BGF bis(2-hydroxyethyl) ether diacrylate (BGF-DEDA). Inside of a 25 mL round bottom flask, TEA (1.6 mL, 11.5 mmol) was added to a solution of BGF-DE (1.34 g, 3.84 mmol) in DCM (7.5 mL). Once cooled near to 0 °C with an ice-water bath, AcrCl (0.75 mL of a 1.23 mol/L solution in DCM) was added dropwise over one hour under vigorous stirring. Afterwards, the flask was left equilibrate to room temperature under stirring for 1 h, and the mixture transferred to a separatory funnel. Once diluted with DCM (10 mL), the mixture was washed with 2 M aqueous H_2SO_4 (3 × 10 mL), 1 M aqueous NaOH (3 × 10 mL) and brine (3 × 10 mL). The organic phase, dried over Na_2SO_4, was filtered on Gooch filter and concentrated under reduced pressure. The residue was purified trough flash column chromatography over

silica gel, with diethyl ether as eluent, giving BGF-DEDA as a pale-yellow liquid, 1.75 g, quantitative yield.

^{1}H NMR (400 MHz, $CDCl_3$) δ (ppm): 6.88–6.64 (m, 6H, Ar—H), 6.47–6.36 (ddd, $J_1 = 1.2$ Hz, $J_2 = 4.8$ Hz, $J_3 = 17.4$ Hz, 2H, -C=CH_2), 6.19–6.10 (m, 2H, (O=)C-CH=C), 5.85–5.80 (m, 2H, C=CH_2), 4.50–4.47 (m, 2H, O-CH_2-C), 4.35–4.31 (m, 2H, O-CH_2-C), 4.27–4.23 (m, 2H, O-CH_2-C), 4.18–4.14 (m, 2H, O-CH_2-C), 3.84–3.76 (m, 8H, Ar-O-CH_3 + Ar-CH_2-Ar).

^{13}C NMR (400 MHz, $CDCl_3$) δ (ppm): 166.2, 150.0, 149.8, 146.8, 146.4, 135.4, 135.3, 134.8, 134.7, 131.3, 131.1, 128.4, 128.3, 121.1, 121.0, 115.0, 114.3, 113.2, 113.0, 71.0, 70.8, 70.0, 69.9, 69.5, 69.3, 69.0, 68.8, 67.7, 63.9, 63.2, 60.5, 56.1, 41.2.

2.2.1.4. Synthesis of bis(2-hydroxyethyl) ether diglycidyl ether (BGF-DGE). Inside a 100 mL round bottom flask, BGF (13.02 g, 50.0 mmol) and TEAB (1.05 g, 5.00 mmol) were dissolved in ECH (39 mL, 500 mmol). The flask was immersed in a pre-heated oil bath at 60 °C for two hours, then was cooled down in an ice-water bath. 50% *w*/w aqueous NaOH (5.0 mL, 200 mmol) was slowly added under vigorous stirring, and the mixture was left stirring overnight at room temperature. DCM (100 mL) and H_2O (100 mL) were added under stirring, then the mixture was transferred to a separatory funnel. After separation of the organic portion, the aqueous phase was further extracted with DCM (50 mL). The combined organic layers, once washed with H_2O (100 mL), were distilled at atmospheric pressure to remove DCM. Afterwards, the application of a reduced pressure ($P = 30$ mmHg, $T_{bath} = 45$ °C) let the distillation of residual ECH. After dehydration with a mechanical pump, BGF-DGE was obtained as a pale yellow solid, quantitative yield.

^{1}H NMR (600 MHz, $CDCl_3$) δ (ppm): 6.88–6.66 (m, 6H, Ar—H), 4.21 (m, 2H, O-CH_2-C*), 4.02 (m, 1H, O-CH_2-C*), 3.85 (s, 2H, Ar-CH_2-Ar), 3.82 (s, 6H, Ar-OCH_3), 3.74 (s, 3H, C(=O)OCH_3), 3.38 (m, 2H, C-C*H(*O*)C), 2.89 (m, 2H, C*(—O—)CH_2), 2.73 (m, 2H, C*(O)CH_2).

^{13}C NMR (600 MHz, $CDCl_3$) δ (ppm): 149.7, 146.4, 134.9, 121.9, 120.9, 115.1, 114.4, 112.8, 112.0, 70.4, 59.2, 50.3, 45.0, 40.9.

2.2.2. Nuclear magnetic resonance spectroscopy (NMR)

^{1}H NMR and ^{13}C NMR spectra were carried out in $CDCl_3$ using a Bruker Avance 600 MHz spectrometer (Bruker, Karlsruhe, Germany) at room temperature at the University of Modena.

2.3. UV-curing process investigation

2.3.1. Formulations preparation

The formulations were prepared by mixing each monomer, either the acrylate (BGF-DEDA) or the epoxy one (BGF-DGE), with 2 phr of their respective photoinitiator. In the BGF-DEDA case, the radical photoinitiator corresponded to the phenylbis(2,4,6-trimethylbenzoyl) phosphine oxide, while for the BGF-DGE monomer, triarylsulfonium hexafluoroantimonate salts, mixed with 50 wt% in propylene carbonate was used. For both the formulations, a first stirring to dissolve the photoinitiator was performed using a sonicator at 50 °C for 60 min. Afterwards, the samples were mixed thoroughly using a planetary Thinky mixer ARE-310 (Laguna Hills, CA, USA) for an additional 10 min.

After mixing, the resin was poured and spread onto a silicon mould to form a uniform layer, and UV-cured under a Dymax lamp for 3 min at 170 mW/cm^2.

In the case of the TEOS-containing formulations, after the UV curing reactions, the material underwent to a thermal process at high temperature (160 °C) for a subsequent 2 h, to achieve a complete conversion of TEOS into SiO_2 particles. The samples were labelled as reported in Table 1.

Table 1
UV-Curable formulations.

TEOS amount [phr]	Acrylate monomer (BGF-DEDA)	Epoxy monomer (BGF-DGE)
0	BGF-DEDA	BGF-DGE
30	BGF-DEDA-3TEOS	BGF-DGE-3TEOS
50	BGF-DEDA-5TEOS	BGF-DGE-5TEOS

2.3.2. Fourier-transform infrared spectroscopy (FTIR)

FTIR spectroscopy was employed to monitor and verify the photocuring behavior of both the acrylate and the epoxy resin formulations. Measurements were performed by means of a Nicolet iS50 spectrometer (Thermo Scientific, Milan, Italy). Both resins exhibited sufficient viscosity to spread a 32 μm-thick layer on a silicon wafer using a stir bar, enabling transmission-mode measurements. This configuration allowed continuous in situ monitoring of reactive group consumption during UV irradiation. In all cases, spectra were collected over the spectral range 4000–600 cm^{-1} at a resolution of 4 cm^{-1}, with 32 scans per measurement.

To obtain real-time curing kinetics, the FTIR spectrometer was equipped with a Hamamatsu Lightingcure LC8 UV lamp operating at 365 nm and 50 mW/cm^2. Spectra were acquired at regular time intervals during UV exposure. The polymerization progress was followed by monitoring the decrease in the C=C stretching vibration of the acrylate peak belonging to BGF-DEDA, centered around 1600 cm^{-1}, and the decrease of the epoxy peak for the BGF-DGE, centered around 900 cm^{-1}. The aliphatic C—H stretching band at approximately 2950 cm^{-1}, which is not involved in the photoreaction, was used as the reference peak.

The ratio of the integrated areas of the acrylate and epoxy peak and the C—H reference peak was calculated at each time point and normalized to its initial value at $t = 0$.

The degree of conversion (%) was then determined according to the equation:

$$Conversion\ (\%) = \frac{\left(\frac{A_{group}}{A_{ref}}\right)_{t=0} - \left(\frac{A_{group}}{A_{ref}}\right)_{t}}{\left(\frac{A_{group}}{A_{ref}}\right)_{t=0}} \times 100$$

where A_{group} represent the integrated areas of the acrylate or epoxy peaks and A_{ref} represent the reference peak. All spectra were processed and baseline-corrected using OMNIC software (Thermo Fisher Scientific), enabling quantification of monomer conversion as a function of UV exposure time.

2.4. Characterization of crosslinked coatings

2.4.1. Dynamic mechanical thermal analysis (DMTA)

Dynamic mechanical thermal analysis (DMTA) was performed using a Triton Technology instrument (Netzsch-Gerätebau GmbH, Selb, Germany) to characterise the thermo-mechanical behavior of the UV-cured materials. Tests were conducted in uniaxial tensile mode at an oscillation frequency of 1 Hz and an initial displacement of 0.02 mm. The temperature used ranged from 0 °C to 150 °C at 5 °C/min; the starting temperature was achieved by cooling the chamber with liquid nitrogen. Testing continued until the sample reached the rubbery plateau region.

Specimens used for the analysis had dimensions of approximately 1.5 × 3.5 × 12 mm. Samples were prepared by pouring the photocurable formulations into silicone moulds, followed by UV curing using a DYMAX ECE flood lamp (Dymax Europe GmbH, Wiesbaden, Germany) at 130 mW/cm^2 intensity for 60s each layer.

The glass transition temperature (T_g) was determined from the maximum peak of the tanδ curve.

2.4.2. SEM analysis

Field-emission scanning electron microscopy (FESEM) was performed using a SUPRA 40 (Zeiss, Oberkochen, Germany) microscope. The specimens were prepared by covering the exposed surface of the

sample after a brittle fracture with a 7 nm Pt layer. The sample was then placed onto an Aluminium stub and attached with a silver-based adhesive.

2.4.3. Thermogravimetric analysis (TGA)

The thermal stability of the polymer was evaluated by thermogravimetric analysis. The sample was heated from room temperature to 900 °C at a 10 °C/min heating rate under a nitrogen atmosphere to maintain an inert environment.

In this work, TGA analysis was performed using a Mettler Toledo TGA/DSC1 (Milano, Italy) instrument equipped with aluminium oxide crucibles (70 μL). 10 to 15 mg of the sample were weighed and placed in the crucible for the analysis. The thermal stability was evaluated by observing the onset of degradation temperature and the residual weight after the test.

2.4.4. Pencil hardness evaluation

Photocured films were assessed for pencil hardness according to ASTM D3363. The test involved pencils graded from 8B (softest) to 8H (hardest). The assigned hardness grade corresponded to the firmest pencil, producing no surface scratches.

2.4.5. Scratch-adhesion test

To assess the coating resistance to separation from the glass substrates, the adhesion test was carried out according to the BS-EN-ISO-2409:2020 standard. The Elcometer 107 Cross Hatch Cutter was used to evaluate the adhesion of the photocrosslinked coatings on glass substrates. The insert number 3 was used as a cutter to perform the test. The cut areas were carefully visually examined with a viewing lens and were classified according to Table 2, using the images as a guide.

Table 2
classification of adhesion performance.

Classification	Description	The appearance of cross-cut areas from which flaking has occurred [a]
0	The edges of the cuts are completely smooth; none of the squares of the lattice is detached.	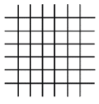
1	Detachment of small flakes of the coating at the intersections of the cuts. A cross-cut area lower than 5% is affected.	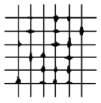
2	The coating has flaked along the edges and/or at the intersections of the cuts. A cross-cut area greater than 5%, but lower than 15%, is affected.	
3	The coating has flaked along the edges of the cuts partly or wholly in large ribbons, and/or it has flaked partly or wholly on different parts of the squares. A cross-cut area greater than 15%, but lower than 35%, is affected.	
4	The coating has flaked along the edges of the cuts in large ribbons and/or some squares have detached partly or wholly. A cross-cut area greater than 35%, but lower than 65%, is affected.	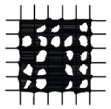
5	Any degree of flaking that cannot even be classified by classification 4	–

3. Results and discussion

3.1. Synthesis of bisguaiacol functionalized resin

The synthesis of functionalized BGF derivatives was articulated in a two-step synthetic protocol for bisguaiacol-F-dyglycidyl ether (BGF-DGE), while bis(2-hydroxyethyl) ether diacrylate (BGF-DEDA) followed a three-step reaction scheme, as reported in Fig. 1. The two synthetic schemes share a common first step.

For the synthesis of ***BGF*** the experimental protocol was based on the procedures reported by Hernandez et al. [34] and their further developments [35–39]. In our synthetic protocol, the acid resin was replaced by SSANa as solid phase catalyst [40]. The product was purified from its higher molecular weight oligomeric fraction (mainly trisphenols, akin to the byproducts of bisphenol F synthesis, [41]. Isomeric purity was determined via ^{1}H NMR spectroscopy, revealing the *p-p'* and *p-m'* isomers ratio to be 80: 20. Even though it has been reported in the literature, [34] we purposedly decided not to perform isomer separation molecules, and thus obtain a less viscous final product.

The following etherification procedure to achieve ***BGF-DE*** was performed on BGF according to previously reported reaction procedures [42,43]. The complex ^{1}H NMR spectrum appearance has been linked to the high reaction temperature which, in presence of atmospheric oxygen, can promote the formation of by-products via oxidative coupling. Those could be potentially avoided by performing the reaction in a sealed vessel under inert atmosphere. However, these conditions would limit the release of the by-produced CO_2, thus reducing the thermodynamic drive of the process. Furthermore, the need for inert atmosphere would severely limit the process' applicability and scale-up feasibility. A blank experiment, namely with BGF and K_2CO_3 only, showed the occurrence of crosslinking phenomena. Initially, the possible isomerization of BGF and derivatives was considered, similarly to what has been reported for bisphenol derivatives [44–48]. Although it has been demonstrated that interconversion phenomena between isomers do not occur in similar conditions [44], it cannot be ruled out that such phenomena could occur under drastic conditions such as those used in the etherification phase. However, the blank experiment dismisses this this possibility, as no interconversion between isomers was recorded via ^{1}H NMR spectroscopy. A tentative purification via chromatography was attempted, which resulted in no improvement in spectral quality. Thus, the material was used as such in the next reaction step.

The acrylation procedure on BGF-DE to synthesize the ***BGF-DEDA*** followed previously established protocols [49]. Although procedures to produce acrylic monomers via transesterification of methyl acrylate under acid-catalyzed conditions are reported, these processes are disadvantageous when applied to the production of difunctional monomers. The low yields of the final product, combined with the need for lengthy and tedious chromatographic purification processes, make the procedure unattractive at present. With the use of AcrCl, the reaction proceeds smoothly, as reported by other protocols. The use of acrylic reagent, the need for a solvent, and a base to suppress the acidity released during the reaction certainly represent a limitation to environmental sustainability. The choice of this protocol was dictated by procedural simplicity.

The synthesis of ***BGF-DGE*** was performed on a batch of BGF that did not undergo purification by column chromatography and followed the reaction protocol established by Hernandez et al., achieving quantitative conversion of the substrate and quantitative yield. Epoxy Equivalent Weight (EEW) was determined according to ASTM D1652, with an average value of 201 g/eq. The discrepancy between the experimental value and the theoretical one (186 g/eq) was attributed to a minor portion of the final product undergoing ring opening phenomena during the workup procedure, thus increasing the corresponding EEW value. The protonic NMR spectrum agrees with those previously reported, with minor baseline fluctuations being attributed to the presence of isomers.

3.2. UV-curing and characterization of biobased coatings

3.2.1. Kinetic studies

The UV curing reactions were deeply investigated by means of both transmission FTIR recorded at different irradiation times. Both pristine and hybrid formulations containing TEOS were studied. Specifically, the radical chain-growth polymerization reaction of BGF-DEDA was investigated by monitoring the acrylate peak centred around 1636 cm^{-1}, while the cationic ring-opening polymerization of BGF-DGE was monitored by following the decrease in the epoxy peak centred around 913 cm^{-1} during irradiation. The conversion was calculated by using **Eq. 1**. As an example, the FTIR spectra collected at different irradiation time are reported respectively for pristine BGF-DEDA and BGF-DGE in Figs. 2 and 3. The final conversion data are collected for all the investigated formulations in Table 2.

Conversion curves as a function of irradiation time are collected in Fig. 4 and 5 respectively for the BGF-DEDA based formulations and BGF-DGE based formulations, both pristine formulations and containing 30 phr and 50 phr TEOS.

The conversion curves clearly show different trend. While for the acrylate monomer the addition of TEOS induced both an enhancement of photopolymerization rate and final double bond conversion, when TEOS is added in the epoxy monomer it induced a decrease of both photopolymerization rate and final epoxy group conversion.

In fact, from data reported in Table 3 it is possible to see that BGF-DEDA reached a final double bond conversion of 74% while the BGF-DGE reached a final epoxy group conversion of 83%, showing good reactivity of these biobased monomers upon UV-Curing process. The addition of TEOS to the photocurable formulations induced an enhancement of double bond conversion for the acrylate resin, which showed a final conversion of 84% in the presence of 30 phr of TEOS and 89% when TEOS was added at 50 phr in the photocurable formulation. On the other hand, the addition of TEOS to BGF-DGE decreased the epoxy group conversion with respect the pristine formulation, reaching a final conversion 69% for the formulation containing 30 phr of TEOS and a very similar conversion (72%) for the formulation containing 50 phr of TEOS.

In the case of the acrylate monomer BGF-DEDA, the enhancement of photopolymerization rate and acrylic double bond conversion could be attributed to a viscosity-lowering effect due to the presence of TEOS (~0.9 mPa·s), which delays diffusion control during rapid radical photopolymerization, allowing a higher reactivity and conversion of acrylate groups [50,51]. On the other hand, when TEOS is added to the epoxy resin, the photogenerated acid could be coordinated by alkoxysilane group competing with epoxy ring in protonation and therefore reducing cationic photocuring rate and the final epoxy conversion.

3.2.2. Thermomechanical and morphological properties

The thermomechanical properties of UV-cured coatings were fully investigated using dynamic mechanical thermal analysis (DMTA). The pencil hardness was measured on UV-cured and dual-cured coatings. Finally, SEM morphological investigation of in-situ generated silica was performed on dual-cured coatings.

The DMTA curves (E' and tanδ curves) are reported in **Fig. 6** and **7** respectively for BGF-DEDA and BGF-DGE and their UV-cured formulations containing TEOS. The T_g of crosslinked coatings was determined as the maximum peak on the tanδ curve. The data are collected in Table 4. It is clear a shifting of tanδ curves to higher temperature by increasing the TEOS content in the photocurable formulations. The T_g of pristine BGF-DEDA was 67 °C and it showed an enhancement to 80 °C and 86 °C respectively for the dual cured coatings achieved in the presence of 30 phr and 50 phr TEOS. The T_g of pristine BGF-DGE was 84 °C and it was increased to 93 °C and 106 °C by increasing the TEOS content in the photocurable formulations of respectively 30 phr and 50 phr.

These data clearly show the good thermo-mechanical properties of the UV-cured biobased resin, attributable to their aromatic structure which confer a quite high T_g. The T_g enhancement in the presence of TEOS could be attributed to the expected silica formation during thermal treatment. The silica generated in-situ hinders the polymer chain mobility with a consequent increase of T_g values for the dual-cured coatings.

The thermo-mechanical performance achieved in this study is notable, with glass transition temperatures (Tg) ranging from 84 °C to 106 °C for the diacrylate and diepoxy resins, respectively, when crosslinked in the presence of 50 phr of TEOS. Although these values do not reach the higher thermo-mechanical properties reported for crosslinked bisphenol-F diepoxy resins, typically exhibiting Tg values between 120 and 180 °C, elastic moduli of 1.5–3 GPa, and tensile strengths of 50–80 MPa [52], such performance is generally obtained through thermal curing. To date, there are no reports describing the UV-curing of bisphenol-F epoxy resins.

Achieving a Tg of 106 °C remains a significant result, particularly considering the use of a bio-based precursor. In our previous work on the UV-curing of diglycidyl furfuryl alcohol, the development of hybrid

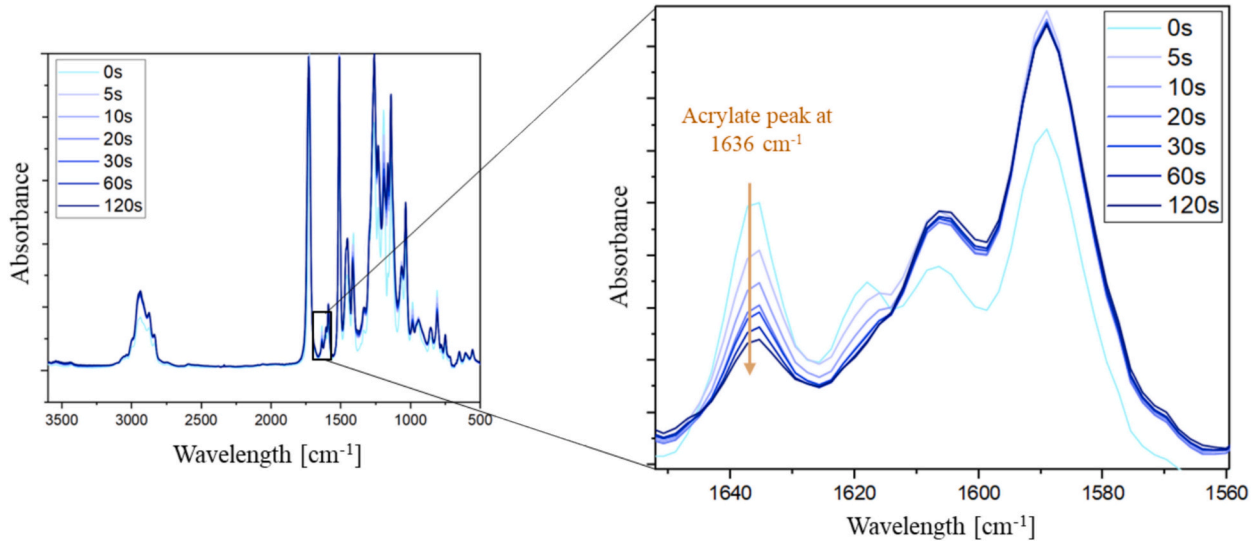

Fig. 2. FTIR spectra collected for the BGF-DEDA pristine formulation after different irradiation time. The left image shows the entire FTIR spectrum, while the right image shows the magnified region corresponding to the acrylate peak.

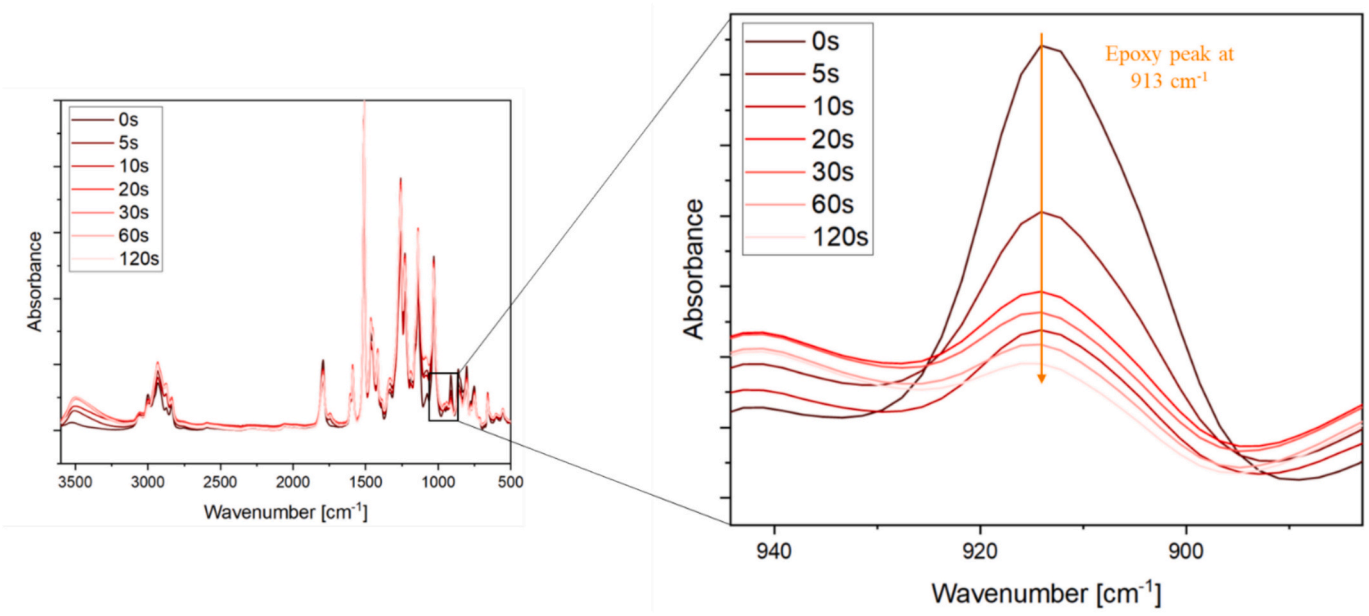

Fig. 3. FTIR spectra collected for the BGF-DGE pristine formulation. The left image shows the entire FTIR spectrum, while the right image shows the magnified region corresponding to the epoxy peak.

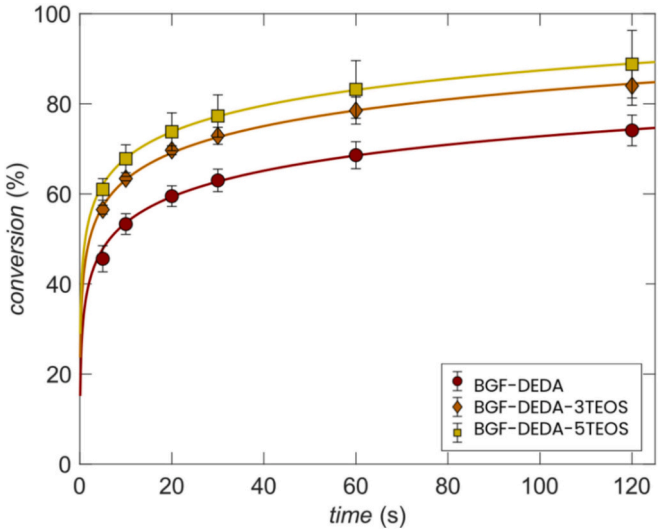

Fig. 4. Conversion curves as function of irradiation time for BGF-DEDA pristine formulation and for BGF-DEDA-3TEOS and BGF-DEDA-5TEOS.

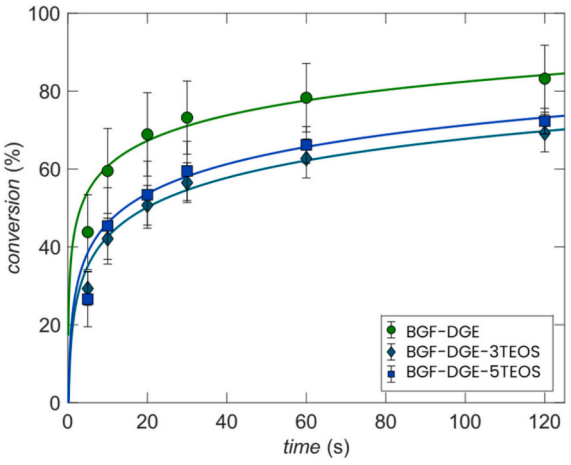

Fig. 5. Conversion curves as function of irradiation time for BGF-DGE pristine formulation and for BGF-DGE-3TEOS and BGF-DGE-5TEOS.

organic–inorganic coatings demonstrated a clear enhancement in modulus, Tg, and hardness. Specifically, the Tg increased from 80 °C for the pristine epoxy-furan coating to 106 °C for the formulation containing 50 phr of TEOS [26]. These findings are consistent with the improvements observed in the present study.

The effect of T_g enhancement due to the in-situ silica formation on surface hardness of crosslinked coatings was evaluated by pencil hardness test. Both BGF-DEDA and BG-DGE UV-cured coatings showed a surface hardness of H. The dual cured coatings evidenced an important increase on surface hardness respectively of 4H and 5H for BGF-DEDA-3TEOS and BGF-DEDA-5TEOS. The epoxy based cured coatings showed even a higher enhancement when dual-cured in the presence of TEOS, showing a surface hardness of 6H and 8H respectively for the coatings BGF-DGE-3TEOS and BGF-DGE-5TEOS. The important enhancement on surface hardness for dual-cured coatings could be attributed to the silica generated in-situ from TEOS that induced a surface hardness enhancement due to the stiffening effect. This is an important result when designing biobased UV-cured coatings as protective coatings.

Table 3
FTIR final conversion for all the investigated photocurable formulations.

Sample name	Acrylic d.b. conv. [%] BGF-DEDA	Sample name	Epoxy conv. [%] BGF-DGE
BGF-DEDA	74 ± 3	BGF-DGE	83 ± 9
BGF-DEDA-3TEOS	84 ± 4	BGF-DGE-3TEOS	69 ± 5
BGF-DEDA-5TEOS	89 ± 8	BGF-DGE-5TEOS	72 ± 3

All the UV-Cured formulations showed a good adhesion properties on glass substrate, showing always edges of the cuts, after the scratch test, completely smooth with none of the squares of the lattice detached (Classification 0 of Table 2). This means that the Uv-Cured coatings showed good adhesion performance on polar substrates such as glass.

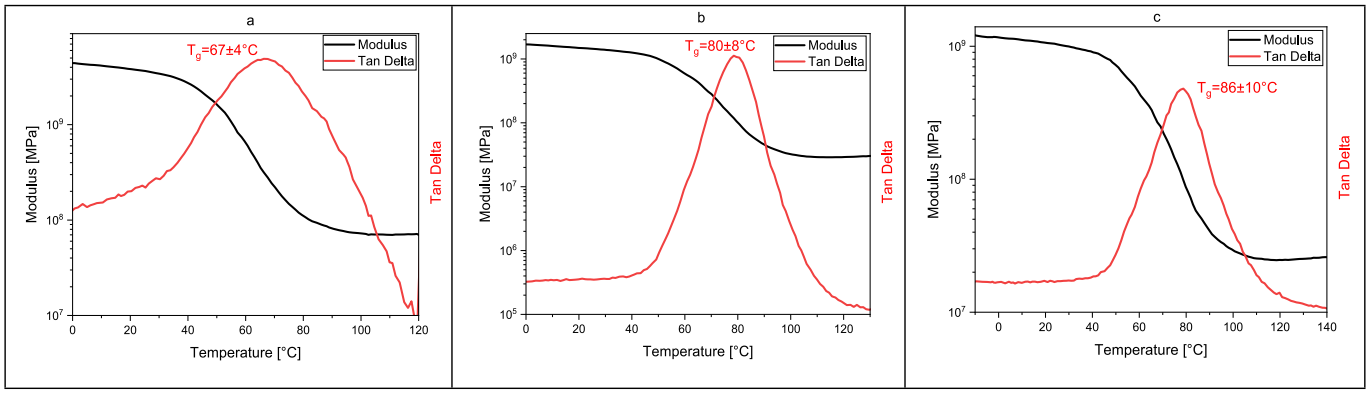

Fig. 6. DMTA curves (E' and tanδ) for UV-cured coating BGF-DEDA (a) and for dual-cured coating BGF-DEDA-3TEOS (b), BGF-DEDA-5TEOS (c).

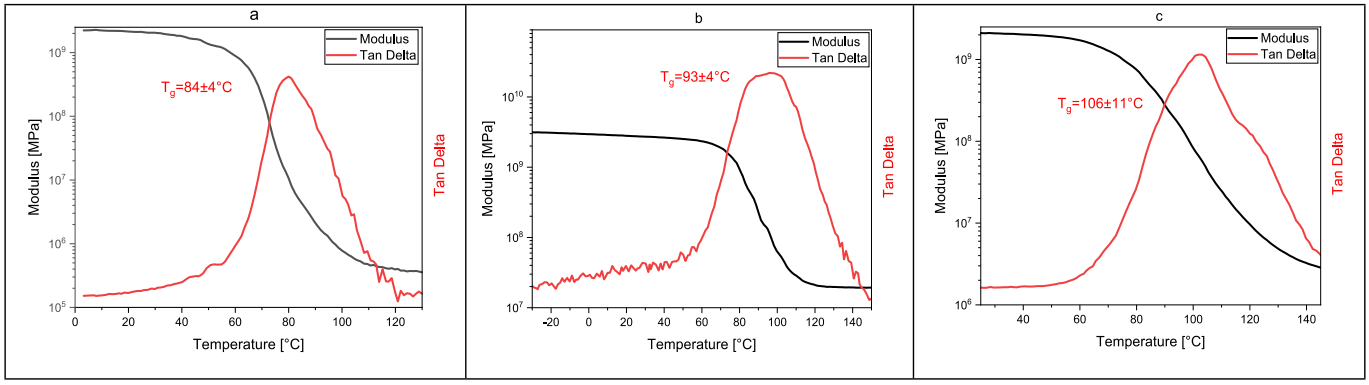

Fig. 7. DMTA curves (E' and tanδ) for UV-cured coating BGF-DGE (a) and for dual-cured coating BGF-DGE-3TEOS (b), BGF-DGE-5TEOS (c).

Table 4
T_g and pencil hardness of UV-cured and dual-cured coatings.

Sample name	Tg by DMTA (°C)	Pencil hardness
BGF-DEDA	67 ± 4	H
BGF-DEDA-3TEOS	80 ± 8	4H
BGF-DEDA-5TEOS	86 ± 10	5H
BGF-DGE	84 ± 4	H
BGF-DGE-3TEOS	93 ± 4	6H
BGF-DGE-5TEOS	106 ± 11	8H

3.2.3. Thermogravimetric evaluation

TGA was performed on all formulations to evaluate the thermal resistance of the composite materials. The results are shown in Fig. 8. Analysis of the data reveals that the polymeric phase is fully degraded after heating in an inert atmosphere to 900 °C, leaving a residual mass composed only of the reinforcing SiO_2 phase, which remains stable under these conditions. Notably, the residual mass percentage decreases with increasing TEOS content in the formulation, likely due to incomplete hydrolysis and condensation of excess TEOS precursor.

3.2.4. Morphological characterization

To further confirm the formation of SiO_2 particles during dual-curing process in the presence of TEOS, morphological FESEM analysis was performed on a fracture surface of the coatings. The FESEM images are reported in Fig. 9 for BGF-DEDA-5TEOS (a) and BGF-DGE-5TEOS (b).

The FESEM images show the formation of particles on the sample surface. The distribution of the spherical nanoparticles (average dimension 398 ± 80 nm) was quite homogeneous without important agglomerations.

4. Conclusions

This work demonstrates the successful development of bio-based UV-curable coatings derived from lignin-based aromatic building blocks, namely bisguaiacol F (BGF) isomers obtained from vanillyl alcohol and guaiacol. Through tailored functionalization strategies, bisguaiacol-F-diacrylate (BGF-DEDA) and bisguaiacol-F-diglycidyl ether (BGF-DGE) and were prepared and systematically investigated in both pristine UV-curable formulations and TEOS-containing hybrid formulations. The photopolymerization studies revealed distinct reactivity trends depending on the curing mechanism: The presence of TEOS enhanced the radical curing of the acrylate system by reducing viscosity and delaying diffusion-controlled termination, whereas it partially hindered the cationic curing of the epoxy resin due to competitive coordination with epoxy ring of photogenerated acid species. Nevertheless, dual-curing strategies enabled effective inorganic network formation, as confirmed by DMTA and FESEM analyses. The in-situ generation of silica during thermal treatment significantly restricted polymer chain mobility, leading to marked T_g enhancements in both acrylate- and epoxy-based systems, with values reaching up to 106 °C. Moreover, the homogeneous distribution of silica nanoparticles contributed to remarkable improvements in surface hardness, achieving up to 8H in epoxy-based hybrid coatings. These findings highlight the strong potential of lignin-derived aromatic platforms for the design of high-performance hybrid materials. Importantly, this study underscores the value of developing bio-based coatings whose final thermo-mechanical properties can be finely tuned, enabling the achievement of high glass transition temperatures and elevated surface hardness, features that are particularly attractive for advanced protective coating applications.

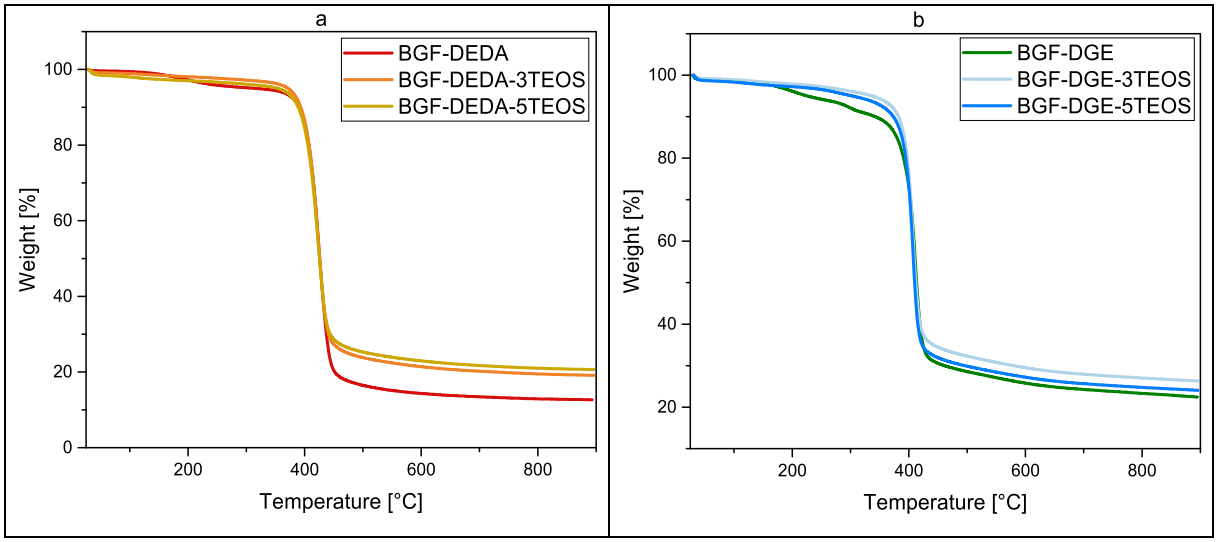

Fig. 8. TGA data performed on to BGF-DEDA formulations (a), and BGF-DGE formulations (b).

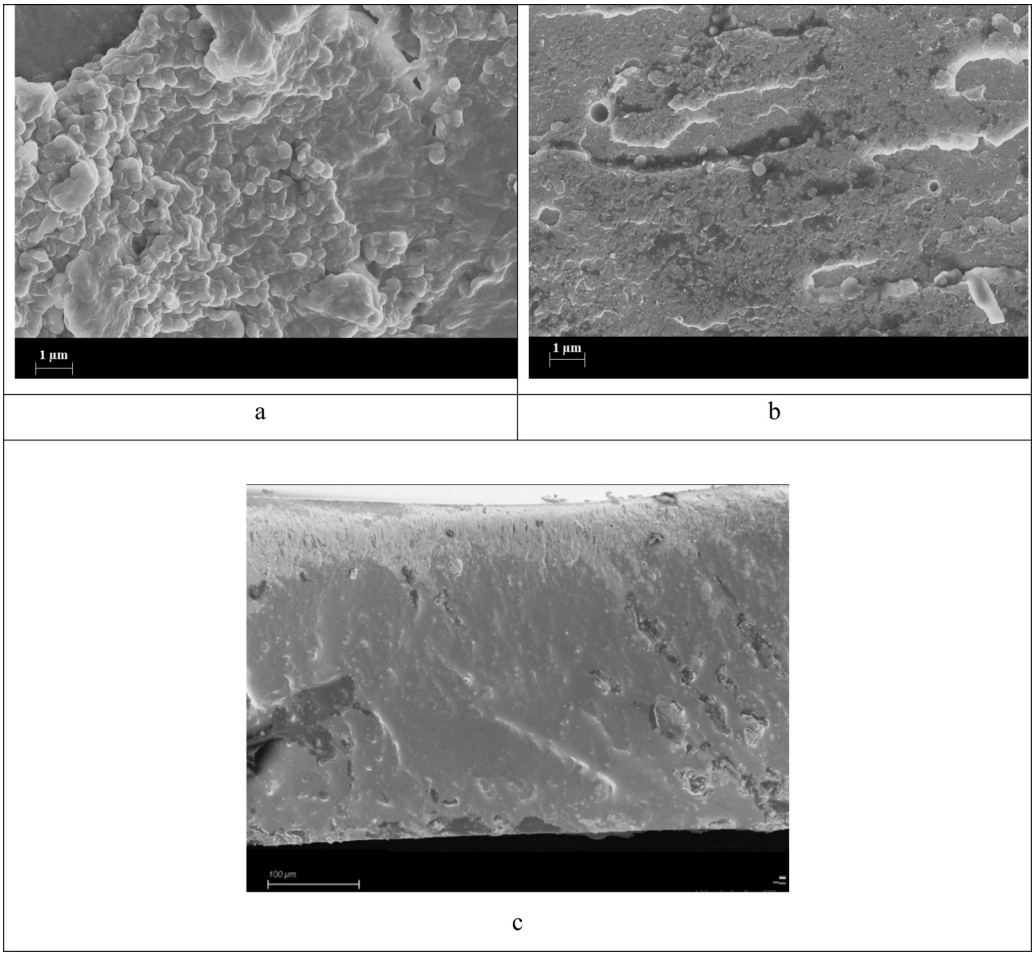

Fig. 9. FESEM images of surface fracture surfaces of the coatings BGF-DEDA-5TEOS (a) and BGF-DGE-5TEOS (b). Cross-sectional morphology for DGE-5TEOS (c).

CRediT authorship contribution statement

Nicola Porcelli: Investigation, Data curation. **Matteo Bergoglio:** Methodology, Formal analysis, Data curation. **Niccolò Braidi:** Formal analysis, Data curation. **Fabrizio Roncaglia:** Conceptualization. **Marco Sangermano:** Project administration, Methodology, Conceptualization.

Author statement

This work introduces, for the first time, the use of lignin-derived

bisguaiacol F (BGF) as a multifunctional platform for UV-curable coating systems, addressing the current lack of studies on its application in this field. Unlike conventional bio-based epoxy resins derived from triglycerides, which suffer from limited thermo-mechanical performance, the rigid aromatic structure of BGF enables the development of high-performance networks. Furthermore the dual functionalization of BGF into both acrylate and epoxy resins, allowing comparison of radical and cationic photopolymerization pathways, combined with the integration of a sol–gel-derived inorganic phase to form hybrid organic–inorganic coatings. This synergistic approach enables the design of largely bio-based UV-curable materials with enhanced thermal and mechanical properties, bridging the gap between sustainability and high-performance coating applications.

Declaration of competing interest

The authors declare that they have no known competing financial interests or personal relationships that could have appeared to influence the work reported in this paper.

Data availability

Data will be made available on request.

References

[1] T. Robert, S. Eschig, M. Sangermano, M. Ocepek, Biobased aromatic building blocks for coating applications, Curr. Opin. Green Sustain. Chem. 49 (2024) 100962, https://doi.org/10.1016/j.cogsc.2024.100962.

[2] I. Fayzullin, A. Gorbachev, S. Volfson, Y. Serikbayev, A. Nakyp, N. Akylbekov, Composite material based on polypropylene and modified natural fillers, Polymers (Basel) 16 (2024) 1703, https://doi.org/10.3390/polym16121703.

[3] L. Xia, T. Gui, J. Wang, H. Tian, Y. Wang, L. Ning, L. Wu, Bio-based coatings: Progress, challenges and future perspectives, Polymers (Basel). 17 (2025) 3266, https://doi.org/10.3390/polym17243266.

[4] W. Zhao, S. Zaman, S. Kong, M. Liu, J. Zou, Z. Zhang, H. Ning, F. Peng, Y. Li, M. Wang, et al., Optimization strategies and diagnostic techniques for water Management in Proton Exchange Membrane Fuel Cells, Green Chemical Engineering 6 (2025) 291–304, https://doi.org/10.1016/j.gce.2024.03.003.

[5] K. Sadeghi, Y. Jeon, J. Seo, Roadmap to the sustainable synthesis of polymers: from the perspective of CO2 upcycling, Prog. Mater. Sci. 135 (2023) 101103, https://doi.org/10.1016/j.pmatsci.2023.101103.

[6] A.B. Scranton, C.N. Bowman, R.W. Peiffer (Eds.), Photopolymerization 673, American Chemical Society, Washington, DC, 1997. ISBN 9780841235205.

[7] M. Sangermano, N. Razza, J.V. Crivello, Cationic UV-curing: technology and applications, Macromol. Mater. Eng. 299 (2014) 775–793, https://doi.org/10.1002/mame.201300349.

[8] L. Pezzana, E. Malmström, M. Johansson, M. Sangermano, UV-curable bio-based polymers derived from industrial pulp and paper processes, Polymers (Basel). 13 (2021) 1530, https://doi.org/10.3390/polym13091530.

[9] M.S. Lima, C.S.M.F. Costa, J.F.J. Coelho, A.C. Fonseca, A.C. Serra, A simple strategy toward the substitution of styrene by Sobrerol-based monomers in unsaturated polyester resins, Green Chem. 20 (2018) 4880–4890, https://doi.org/10.1039/C8GC01214H.

[10] V.J. Patil, S.J. Dhole, V.S. Bhamare, S.S. Bhamare, S.L. Sonawane, V.V. Gite, Bio-based polyester polyurethane acrylate resin: synthesis and application for Solventless UV-curable coatings, React. Funct. Polym. 215 (2025) 106345, https://doi.org/10.1016/j.reactfunctpolym.2025.106345.

[11] L. Xia, T. Gui, J. Wang, H. Tian, Y. Wang, L. Ning, L. Wu, Bio-based coatings: progress, challenges and future perspectives, Polymers (Basel) 17 (2025) 3266, https://doi.org/10.3390/polym17243266.

[12] M. Bergoglio, G. Palazzo, D. Reisinger, M. Porcarello, G. Kortaberria, S. Schlögl, M. Sangermano, Cationic UV-curing of bio-based Epoxidized Castor oil Vitrimers with electrically conductive properties, React. Funct. Polym. 200 (2024) 105936, https://doi.org/10.1016/j.reactfunctpolym.2024.105936.

[13] M. Bergoglio, E. Rossegger, S. Schlögl, T. Griesser, C. Waly, F. Arbeiter, M. Sangermano, Multi-material 3D printing of biobased epoxy resins, Polymers (Basel). 16 (2024) 1510, https://doi.org/10.3390/polym16111510.

[14] S. Subramaniyan, M. Bergoglio, M. Sangermano, M. Hakkarainen, Vanillin-derived thermally reprocessable and chemically recyclable Schiff-base epoxy thermosets, Global Chall. n/a (2023) 2200234, https://doi.org/10.1002/gch2.202200234.

[15] S. Nameer, D.B. Larsen, J.Ø. Duus, A.E. Daugaard, M. Johansson, Biobased Cationically Polymerizable epoxy thermosets from furan and fatty acid derivatives, ACS Sustain. Chem. Eng. 6 (2018) 9442–9450, https://doi.org/10.1021/acssuschemeng.8b01817.

[16] C. Noè, S. Malburet, A. Bouvet-Marchand, A. Graillot, C. Loubat, M. Sangermano, Cationic Photopolymerization of bio-renewable Epoxidized monomers, Prog. Org. Coat. 133 (2019) 131–138, https://doi.org/10.1016/j.porgcoat.2019.03.054.

[17] X. Pan, P. Sengupta, D.C. Webster, High biobased content epoxy–anhydride thermosets from epoxidized sucrose esters of fatty acids, Biomacromolecules 12 (2011) 2416–2428, https://doi.org/10.1021/bm200549c.

[18] Z. Wang, X. Zhang, R. Wang, H. Kang, B. Qiao, J. Ma, L. Zhang, H. Wang, Synthesis and characterization of novel soybean-oil-based elastomers with favorable Processability and tunable properties, Macromolecules 45 (2012) 9010–9019, https://doi.org/10.1021/ma301938a.

[19] M. Chrysanthos, J. Galy, J.-P. Pascault, Preparation and properties of bio-based epoxy networks derived from isosorbide diglycidyl ether, Polymer (Guildf) 52 (2011) 3611–3620, https://doi.org/10.1016/j.polymer.2011.06.001.

[20] L. Pezzana, A. Emanuele, R. Sesana, C. Delprete, E. Malmström, M. Johansson, M. Sangermano, Cationic UV-curing of isosorbide-based epoxy coating reinforced with Macadamia nut Shell powder, Prog. Org. Coat. 185 (2023) 107949, https://doi.org/10.1016/j.porgcoat.2023.107949.

[21] S. Ma, X. Liu, Y. Jiang, Z. Tang, C. Zhang, J. Zhu, Bio-based epoxy resin from Itaconic acid and its thermosets cured with anhydride and Comonomers, Green Chem. 15 (2013) 245–254, https://doi.org/10.1039/C2GC36715G.

[22] L. Pezzana, G. Melilli, M. Sangermano, N. Sbirrazzuoli, N. Guigo, Sustainable approach for coating production: room temperature curing of Diglycidyl Furfuryl amine and Itaconic acid with UV-induced thiol-Ene surface post-functionalization, React. Funct. Polym. 182 (2023) 105486, https://doi.org/10.1016/j.reactfunctpolym.2022.105486.

[23] L. Papadopoulos, L. Pezzana, N.M. Malitowski, M. Sangermano, D.N. Bikiaris, T. Robert, UV-curing additive manufacturing of bio-based thermosets: effect of diluent concentration on printing and material properties of Itaconic acid-based materials, ACS Omega 8 (2023) 31009–31020, https://doi.org/10.1021/acsomega.3c02808.

[24] L. Pezzana, M. Mousa, E. Malmström, M. Johansson, M. Sangermano, Bio-based monomers for UV-curable coatings: Allylation of Ferulic acid and investigation of Photocured thiol-Ene network, Prog. Org. Coat. 150 (2021) 105986, https://doi.org/10.1016/J.PORGCOAT.2020.105986.

[25] F. Hu, J.J. La Scala, J.M. Sadler, G.R. Palmese, Synthesis and characterization of thermosetting furan-based epoxy systems, Macromolecules 47 (2014) 3332–3342, https://doi.org/10.1021/ma500687t.

[26] L. Pezzana, G. Melilli, N. Guigo, N. Sbirrazzuoli, M. Sangermano, Cationic UV curing of bioderived epoxy furan-based coatings: tailoring the final properties by in situ formation of hybrid network and addition of Monofunctional monomer, ACS Sustain. Chem. Eng. 9 (2021) 17403–17412, https://doi.org/10.1021/acssuschemeng.1c06939.

[27] L. Pezzana, G. Melilli, N. Guigo, N. Sbirrazzuoli, M. Sangermano, Cross-linking of biobased Monofunctional furan epoxy monomer by two steps process, UV irradiation and thermal treatment, Macromol. Chem. Phys. 224 (2023), https://doi.org/10.1002/macp.202200012.

[28] C. Xu, R.A.D. Arancon, J. Labidi, R. Luque, Lignin Depolymerisation strategies: towards valuable chemicals and fuels, Chem. Soc. Rev. 43 (2014) 7485–7500, https://doi.org/10.1039/C4CS00235K.

[29] Y. Peng, K.H. Nicastro, T.H. Epps, C. Wu, Evaluation of estrogenic activity of novel bisphenol a alternatives, four bioinspired Bisguaiacol F specimens, by in vitro assays, J. Agric. Food Chem. 66 (2018) 11775–11783, https://doi.org/10.1021/acs.jafc.8b03746.

[30] S.-F. Koelewijn, D. Ruijten, L. Trullemans, T. Renders, P. Van Puyvelde, H. Witters, B.F. Sels, Regioselective synthesis, isomerisation, *in vitro* Oestrogenic activity, and copolymerisation of Bisguaiacol F (BGF) isomers, Green Chem. 21 (2019) 6622–6633, https://doi.org/10.1039/C9GC02619C.

[31] K.H. Nicastro, C.J. Kloxin, T.H. Epps, Potential lignin-derived alternatives to bisphenol a in diamine-hardened epoxy resins, ACS Sustain. Chem. Eng. 6 (2018) 14812–14819, https://doi.org/10.1021/acssuschemeng.8b03340.

[32] J.S. Mahajan, E.R. Gottlieb, J.M. Kim, T.H. Epps, Toward sustainable materials: from lignocellulosic biomass to high-performance polymers, Acc. Mater. Res. 6 (2025) 316–326, https://doi.org/10.1021/accountsmr.4c00359.

[33] Y.-T. Wong, L.T.J. Korley, Engineering lignin-derivable Diacrylate networks with tunable architecture and mechanics, Mater. Adv. 5 (2024) 6070–6080, https://doi.org/10.1039/D4MA00159A.

[34] E.D. Hernandez, A.W. Bassett, J.M. Sadler, J.J. La Scala, J.F. Stanzione, Synthesis and characterization of bio-based epoxy resins derived from Vanillyl alcohol, ACS Sustain. Chem. Eng. 4 (2016) 4328–4339, https://doi.org/10.1021/acssuschemeng.6b00835.

[35] K.M. Hambleton, J.F. Stanzione, Synthesis and characterization of a low-molecular-weight Novolac epoxy derived from lignin-inspired Phenolics, ACS Omega 6 (2021) 23855–23861, https://doi.org/10.1021/acsomega.1c02799.

[36] A.M. Chong, S.A. Salazar, J.F. Stanzione III, Multifunctional biobased Benzoxazines blended with an epoxy resin for tunable high-performance properties, ACS Sustain. Chem. Eng. 9 (2021) 5768–5775, https://doi.org/10.1021/acssuschemeng.1c01338.

[37] S. Curia, A. Biundo, I. Fischer, V. Braunschmid, G.M. Gübitz, J.F. Stanzione, Towards sustainable high-performance thermoplastics: synthesis, characterization, and enzymatic hydrolysis of Bisguaiacol-based polyesters, ChemSusChem 11 (2018) 2529–2539, https://doi.org/10.1002/cssc.201801059.

[38] Y.-T. Wong, L.T.J. Korley, Engineering lignin-derivable Diacrylate networks with tunable architecture and mechanics, Mater. Adv. 5 (2024) 6070–6080, https://doi.org/10.1039/D4MA00159A.

[39] K.H. Nicastro, C.J. Kloxin, T.H. Epps, Potential lignin-derived alternatives to bisphenol a in diamine-hardened epoxy resins, ACS Sustain. Chem. Eng. 6 (2018) 14812–14819, https://doi.org/10.1021/acssuschemeng.8b03340.

[40] F. Roncaglia, L. Forti, S. D'Anna, L. Maletti, An expedient catalytic process to obtain Solketal from biobased glycerol, Processes 9 (2021) 141, https://doi.org/10.3390/pr9010141.
[41] S.K. Jana, T. Kugita, S. Namba, Aluminum-grafted MCM-41 molecular sieve: an active catalyst for bisphenol F synthesis process, Appl. Catal. A Gen. 266 (2004) 245–250, https://doi.org/10.1016/j.apcata.2004.02.013.
[42] Y. Wang, Y. Wang, X. Li, J. Zhao, Etherification of biobased resveratrol with ethylene carbonate and its crosslinked Polymethacrylates, Mater. Chem. Phys. 316 (2024) 129121, https://doi.org/10.1016/j.matchemphys.2024.129121.
[43] X. Guo, F. Gao, F. Chen, J. Zhong, L. Shen, C. Lin, Y. Lin, Dynamic enamine-one bond based Vitrimer via amino-Yne click reaction, ACS Macro Lett. 10 (2021) 1186–1190, https://doi.org/10.1021/acsmacrolett.1c00550.
[44] S.-F. Koelewijn, D. Ruijten, L. Trullemans, T. Renders, P. Van Puyvelde, H. Witters, B.F. Sels, Regioselective synthesis, isomerisation, *in vitro* Oestrogenic activity, and copolymerisation of Bisguaiacol F (BGF) isomers, Green Chem. 21 (2019) 6622–6633, https://doi.org/10.1039/C9GC02619C.
[45] S. Van de Vyver, S. Helsen, J. Geboers, F. Yu, J. Thomas, M. Smet, W. Dehaen, Y. Román-Leshkov, I. Hermans, B.F. Sels, Mechanistic insights into the kinetic and Regiochemical control of the thiol-promoted catalytic synthesis of Diphenolic acid, ACS Catal. 2 (2012) 2700–2704, https://doi.org/10.1021/cs300635r.
[46] J.R. Campbell, US Pat, 4156790, 1979.
[47] F. Oi, N. Yanase, M. Yamamoto US Pat. 6861562 (2005) B2.
[48] U. Rudolph, C. Wulff US Pat, 5015784, 1991.
[49] X. Yang, S. Lu, Y. Zhang, H. Xu, X. Cai, C. Shu, DABSO-mediated Hydrosulfonylation of activated alkenes, Org. Lett. 27 (2025) 4927–4932, https://doi.org/10.1021/acs.orglett.5c01170.
[50] M. Harsch, J. Karger-Kocsis, M. Holst, Influence of fillers and additives on the cure kinetics of an epoxy/anhydride resin, Eur. Polym. J. 43 (2007) 1168–1178, https://doi.org/10.1016/j.eurpolymj.2007.01.025.
[51] J.R. Nowers, B. Narasimhan, The effect of interpenetrating polymer network formation on polymerization kinetics in an epoxy-acrylate system, Polymer (Guildf). 47 (2006) 1108–1118, https://doi.org/10.1016/j.polymer.2005.12.030.
[52] I.V. Tarasov, A.V. Oboishchikova, R.S. Borisov, V.V. Kireev, I.S. Sirotin, Phosphazene-containing epoxy resins based on bisphenol F with enhanced heat resistance and mechanical properties: synthesis and properties, Polymers 14 (21) (2022) 4547, https://doi.org/10.3390/polym14214547, 27. (PMID: 36365541; PMCID: PMC9655627).